INAF
ISTITUTO NAZIONALE DI ASTROFISICA
OSSERVATORIO ASTROFISICO DI ARCETRI
UNIVERSITÀ DEGLI STUDI FIRENZE

Lecture VI: the Interstellar Medium of galaxies

Astrophysics of Galaxies 2019-2020

Stefano Zibetti - INAF Osservatorio Astrofisico di Arcetri

Lecture VI

The multi-phase ISM

constituents of ISM in Milky Way	where	temperature density ...	how observed
atomic hydrogen HI	in disk, some in halo $\approx 90\%$ of mass, 50% of vol.	$50...300$K $1...100$cm^{-3}	21cm radio line UV absorption lines
molecular hydrogen H_2	dark clouds in disk $\approx 10\%$ of mass, 1% of vol.	$3...100$K $10^2...10^6$cm^{-3}	UV absorption lines IR emission lines
other molecules CO, HCN, H_2O ...	dark clouds in disk	$3...100$K $10^2...10^6$cm^{-3}	radio and IR emission
ionized hydrogen HII	near hot stars, emission nebulae	$5000...10000$K $10^2...10^4$cm^{-3}	optical and IR emission lines, radio continuum
hot gas	everywhere	$10^6...10^7$K 0.01cm^{-3}	X-ray emission
dust grains	mostly in disk $\approx 1\%$ of mass	$20...100$K size ≈ 2000Å	reddening/absorption of starlight, IR emission
magnetic fields	everywhere	μGauss	polarization of stars, Zeeman effect, synchrotron radiation
cosmic rays	everywhere	energies up to 10^{20}eV	air showers

The total mass of the ISM in the Milky Way amounts to ≈ 15% of the mass in stars, which is a typical value for spiral galaxies in general.

The diffuse InterStellar Medium

The existence of the diffuse ISM was first recognized by the observation of absorption lines in binary stars. Most lines moved back and forth due to the motion of the stars around each other but some lines didn't move (like CaI and NaI lines). These were due to intervening gas between the binary and the observer. The analysis of the stationary lines shows that they are composed of several narrower lines which shows that the gas is clumpy. Satellite observations of blue stars show a large variety of **interstellar UV absorption lines of Lyα, N, O, Mg, Si, S, Ar, Fe** which allow to determine the metal abundance of the ISM. The abundances in the gas turn out to somewhat lower than in the sun. Moreover, some heavy elements (those with low ionization energies or high condensation temperatures, like Ca and Fe) are significantly depleted. They condense onto dust particles.

IMPRS Astrophysics Introductory Course - Credits Ralf Bender et al.

Neutral atomic Hydrogen: HI

- Traced in emission by 21 cm line (1420 GHz)
- Spin-flip transition: atomic transition of an electron between the two hyperfine levels of the hydrogen 1s ground state that have an energy difference of ~ 5.87433 μeV
- Highly forbidden transition: life-time ~11 Myr!
- Excited by collisions:
  - mean free path $l_c \approx (n_H \sigma_c)^{-1} = \frac{10^{15}}{n_H} \mathrm{cm}$
  - typical velocity $\frac{3}{2} m_H v^2 = k_B T$
  - collision rate $\tau_c^{-1} = \frac{v}{l_c} = \left(\frac{2k_B T}{3m_H}\right)^{1/2} n_H \sigma_c = 7 \cdot 10^{-12} n_H T^{1/2} s^{-1}$

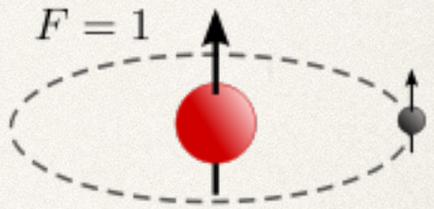

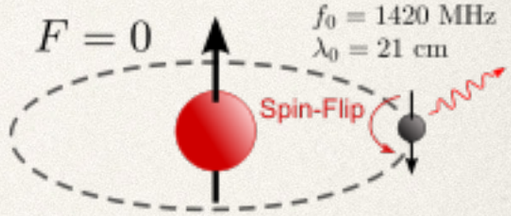

- In typical conditions T~10-100K and n_H~1 cm^{-3}, resulting in τ_c~500 yr, much shorter than the life-time
- Hence the equilibrium is established by the collisions using the Boltzmann equation $N_1/N_0 = e^{-\frac{E_{01}}{kT}}$

  but since $E_{01} << kT$ the levels are equally populated, so the number of atom that can make the transition are $n_H/2$
- If we integrate over the volume of (part) of a galaxy [or work out the column density], it turns out that the large number of atoms available for the transition compensates the very long transition time
- In fact, the 21cm emission is detected! First time in our Galaxy in 1951 after the prediction by van der Hulst in 1944

HI detection via absorption: Lyα absorbers

- Use background beacon sources with smooth spectra (e.g. QSOs) to peer through the HI clouds
- Different class of absorbers, depending of HI column density:
  - Lyα-forest absorbers: N(HI)<10^{17} cm^{-2}
  - Lyα-limit systems: optically thick at the Lyman limit, 10^{17} cm^{-2}<N(HI)<2 10^{20} cm^{-2}
  - Damped-Lyα (DLA) systems: damping wings are optically thick, N(HI)>2 10^{20} cm^{-2}
    Mostly neutral gas!

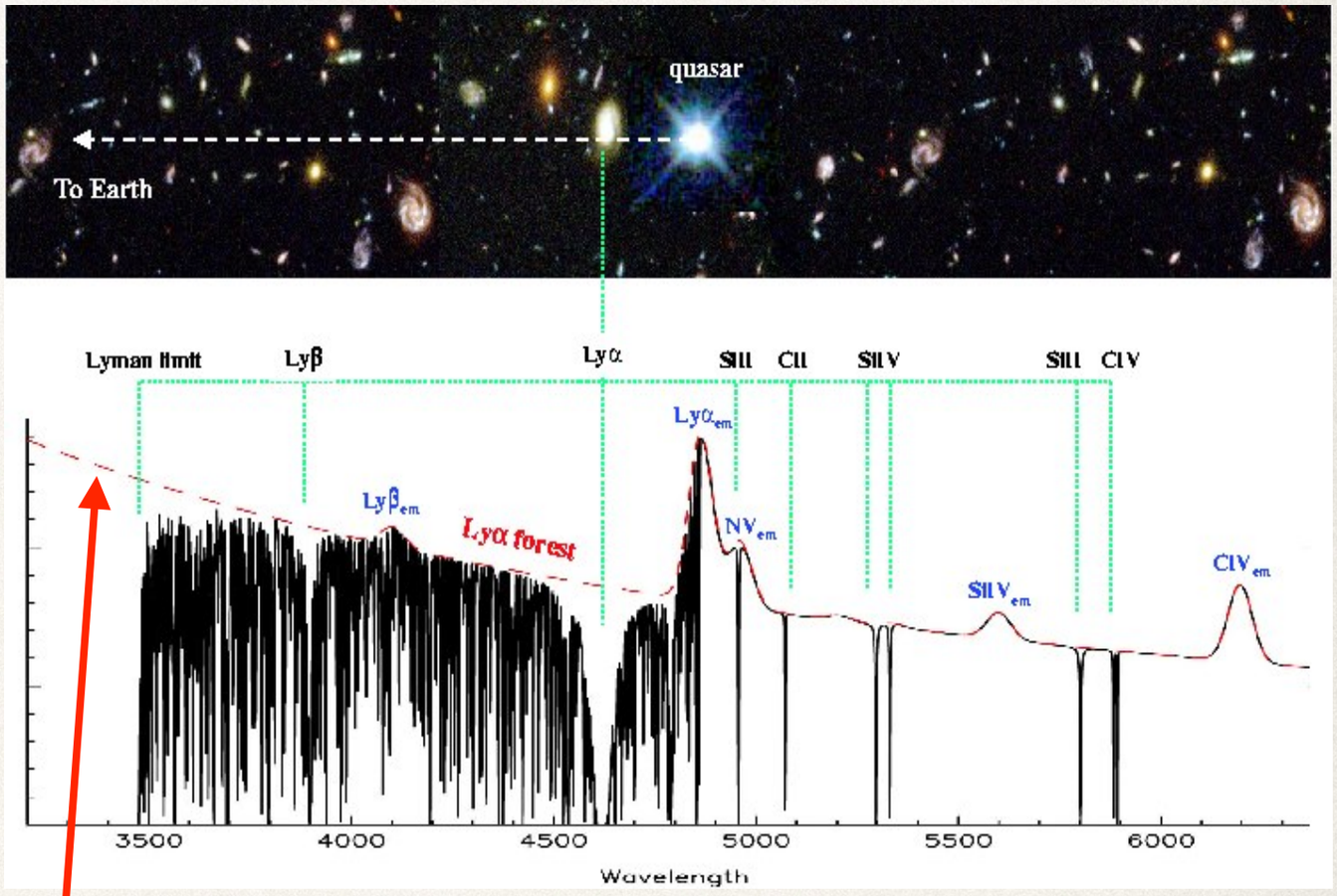

emitted spectrum by background QSO, redshifted by $(1 + z_{em})$

Intervening clouds remove photons at the restframe λ of the Lyα

In the observer's frame this translates into absorptions at $\lambda_{abs} = \lambda_{Ly\alpha}(1 + z_{abs})$

Molecular Hydrogen H_2 / Gas

- Recall molecules have 3 kind of transitions / spectra:
  - electronic
    - vibrational
      - roto-vibrational
- The vibrational and roto-vibrational transitions are extremely unlikely for molecules without permanent electric dipole, as they are accessible only through quadrupolar transitions.
  - H2, as a homonuclear molecule, has no electric dipole so that rotovibrational transitions in the ground electronic state are all forbidden.
  - The first allowed dipole transitions from the ground state occur at energies between 11 and 14 eV (in the UV) and are known as Lyman and Werner bands. Hence they require a relatively high temperature to be excited efficiently.
  - Also, such a hard UV cannot be accessed from the ground
  - How to trace H_2???

Eisberg & Resnick, Quantum Physics

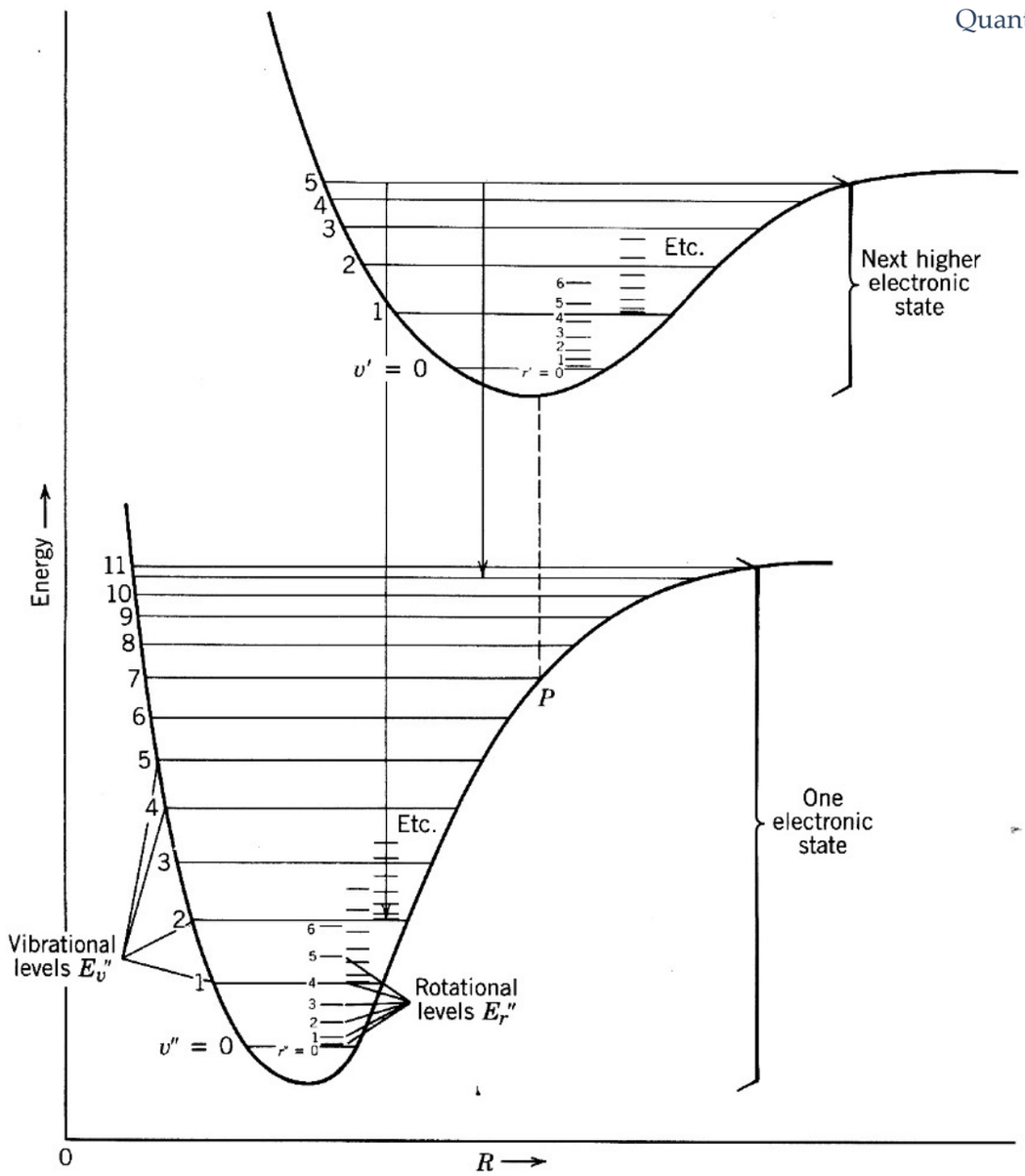

Figure 12-9 Illustrating the molecular energy versus internuclear separation curves for two electronic states. Each electronic state has its own set of vibrational levels, and each vibrational level has its own set of rotational levels.

CO as molecular gas tracer

- CO has a permanent electric dipole, so roto-vibrational transitions are allowed in the ground level

$$E_J = \frac{\hbar^2}{2I} J(J+1), \quad \Delta J = \pm 1$$

$$\Delta E_J = E_J - E_{J-1} = \frac{\hbar^2}{2I}\left[J(J+1)-(J-1)J\right] = \frac{\hbar^2}{2I} J \approx J\cdot(10^{-4}\text{–}10^{-3} eV)$$

- Typical transition energy is in the mm regime

- When density too high for ^{12}CO to be optically thin, use ^{13}CO

Lines of different J-transitions are evenly spaced in frequency

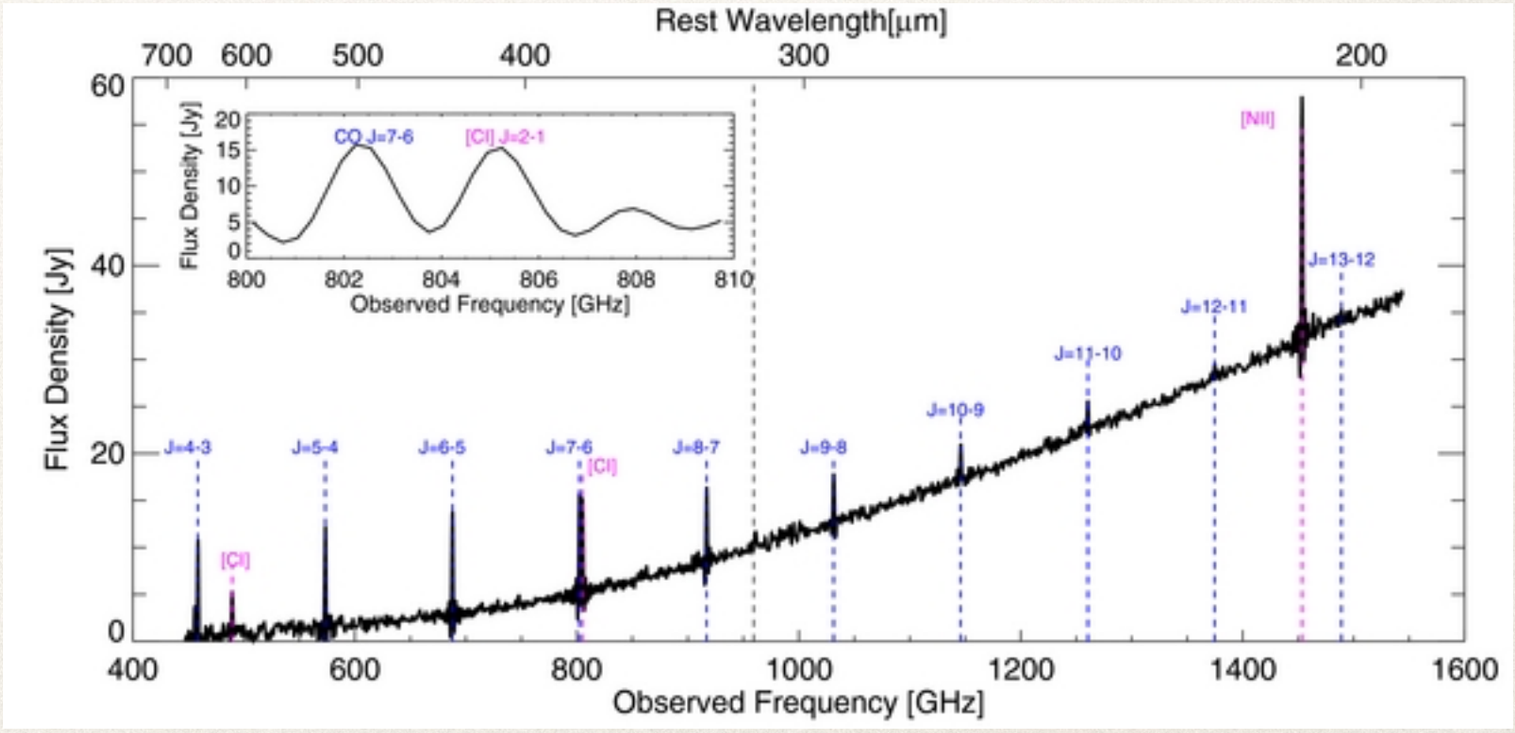

NGC7552 (Rosenberg+2015)

CO-to-H_2 conversion

- It's a whole topic in the astrophysical literature, with the conversion factor often referred to as α_{CO}
  - Indirectly calibrated using dust and making assumptions on some parameter not to depend on metallicity

e.g. Leroy et al. (2011):

We and assume that dust and gas are linearly related by a gas-to-dust ratio, δ_{GDR}, so that

$$\delta_{GDR}\ \Sigma_{dust} = \Sigma_{H2} + \Sigma_{HI}\ . \quad (1)$$

where Σ_{dust}, Σ_{H2}, and Σ_{HI} are the mass surface densities of dust, H_2, and H I along a line of sight. Substituting $\Sigma_{H2} = \alpha_{CO}\ I_{CO}$ we have

$$\delta_{GDR}\ \Sigma_{dust} = \alpha_{CO}\ I_{CO} + \Sigma_{HI}\ , \quad (2)$$

where the CO-to-H_2 conversion factor, α_{CO}, and gas-to-dust ratio, δ_{GDR}, are unknown and Σ_{dust}, I_{CO}, and Σ_{HI} are measured. After assembling Σ_{dust}, I_{CO}, and Σ_{HI} over many lines of sight in a region, we will use these data to solve for α_{CO} that best allows a single δ_{GDR} to describe the data.

The CO ladder

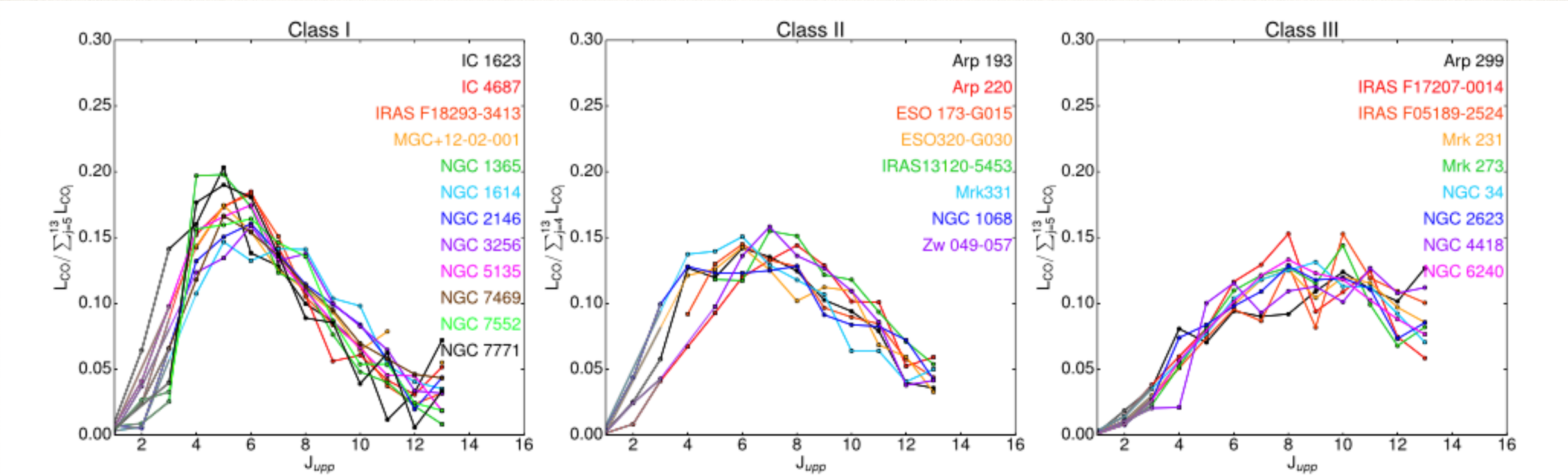

- Different Spectral Line Energy Distributions (SLEDs) denote different temperatures, as the population of different rotational states depends on T

THEORY OF ISM

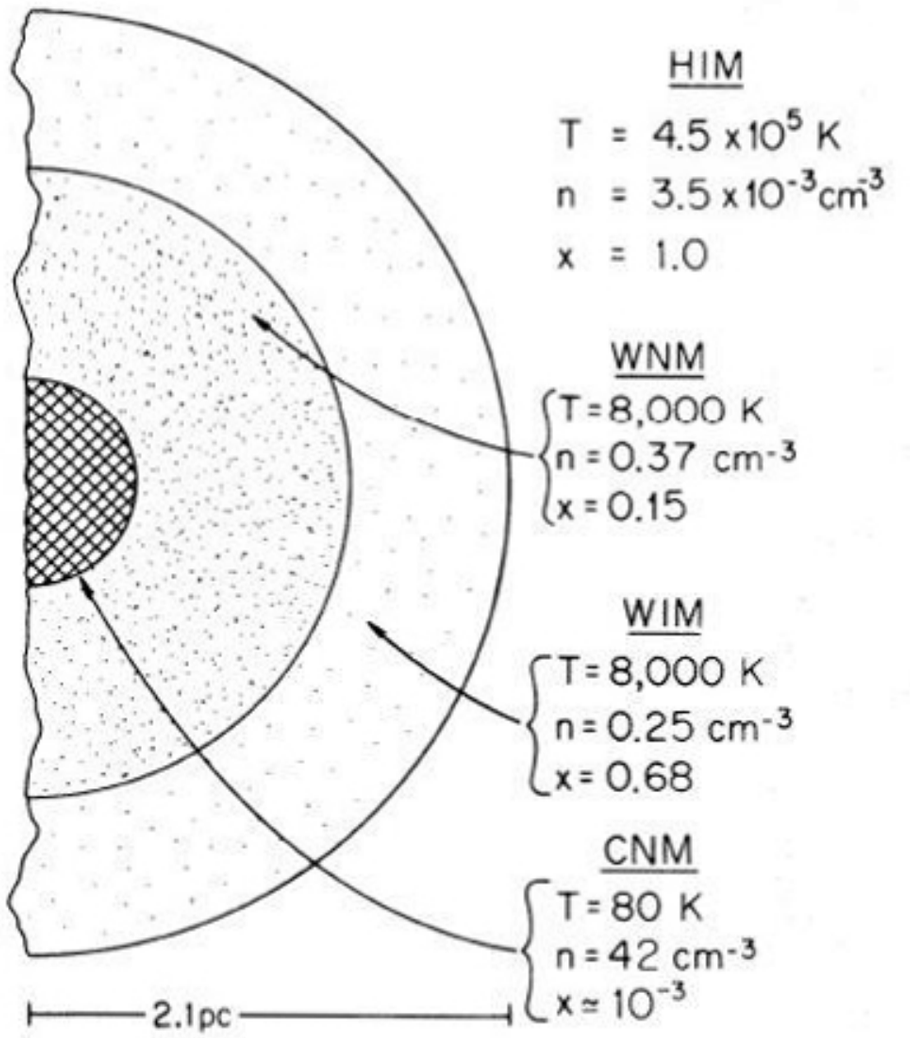

FIG. 1

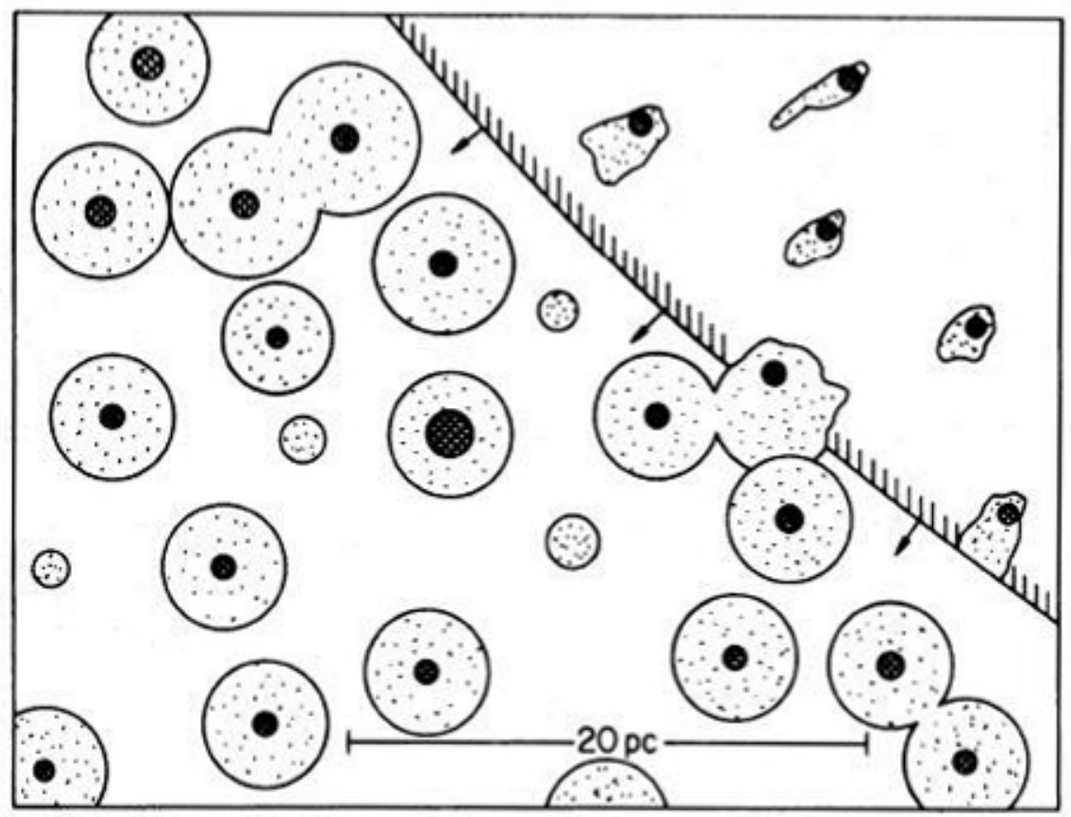

FIG. 2

FIG. 1.—Cross section of a characteristic small cloud. The crosshatched region shows the cold core, which gives the usual optical absorption lines. Next is the warm neutral medium (WNM) with ionization produced by soft X-ray background. The outer layer (WIM) is gas largely ionized by stellar UV background. Typical values of hydrogen density n, temperature T, and ionization $x = n_e/n$ are shown for each component, except that a higher than average value of the soft X-ray flux has been assumed in order to produce a significant amount of WNM at this pressure.

FIG. 2.—Small-scale structure of the interstellar medium. A cross section of a representative region 30 pc × 40 pc in extent is shown, with the area of the features being approximately proportional to their filling factors. A supernova blast wave is expanding into the region from the upper right. The radius of the neutral cores of the clouds (represented by crosshatching) ranges from about 0.4 to 1 pc in this small region; all the clouds with cores have warm envelopes (*dotted regions*) of radius $a_w \sim 2.1$ pc. A few clouds are too small to have cores. The envelopes of clouds inside the SNR are compressed and distorted.

HI clouds

The typical size of an HI cloud is R ≈ 5pc and a typical mass is M ≈ 500 M_Θ. If we calculate the internal energy of the cloud:

$$U \approx \frac{3Mk_BT}{2m_H} \approx 10^{46} ergs$$

this turns out to be larger than the potential energy:

$$E_G \approx \frac{GM^2}{R} \approx 3 \cdot 10^{45} ergs$$

which implies that the HI clouds are not gravitationally bound (Virial theorem: $|U| = |E_G/2|$). This means that the clouds can only be stable if they are in pressure equilibrium with their environment.

(credits to Ralf Bender et al.)

Molecular clouds

The high density molecular clouds were first detected as dark globules which absorb the light of stars in the Milky Way. The main content of the molecular clouds, namely H_2 molecules can not be detected easily in the radio and, so, these clouds were first surveyed based on radio emission of the CO molecule (rotational transition from J=1 to J=0 corresponding to 2.6mm wavelength). The CO also has the advantage that in very dense clouds, the ^{13}CO isotope which is about 40 times less abundant than ^{12}CO, still allows to observe regions which are optically thick in ^{12}CO.

Other molecules detected range from water (H_2O) and cyanide (HCN) to more complex molecules such as ethyl alcohol (CH_3CH_2OH). In fact, hundreds of such molecules have been found in molecular clouds and identified by comparing their radio emission line spectra with radio spectra of the same molecules in laboratories on Earth. By analyzing the ratios of radio spectral lines from the molecular clouds, we find that the gas there is extremely cold - ranging from about 3-20 K.

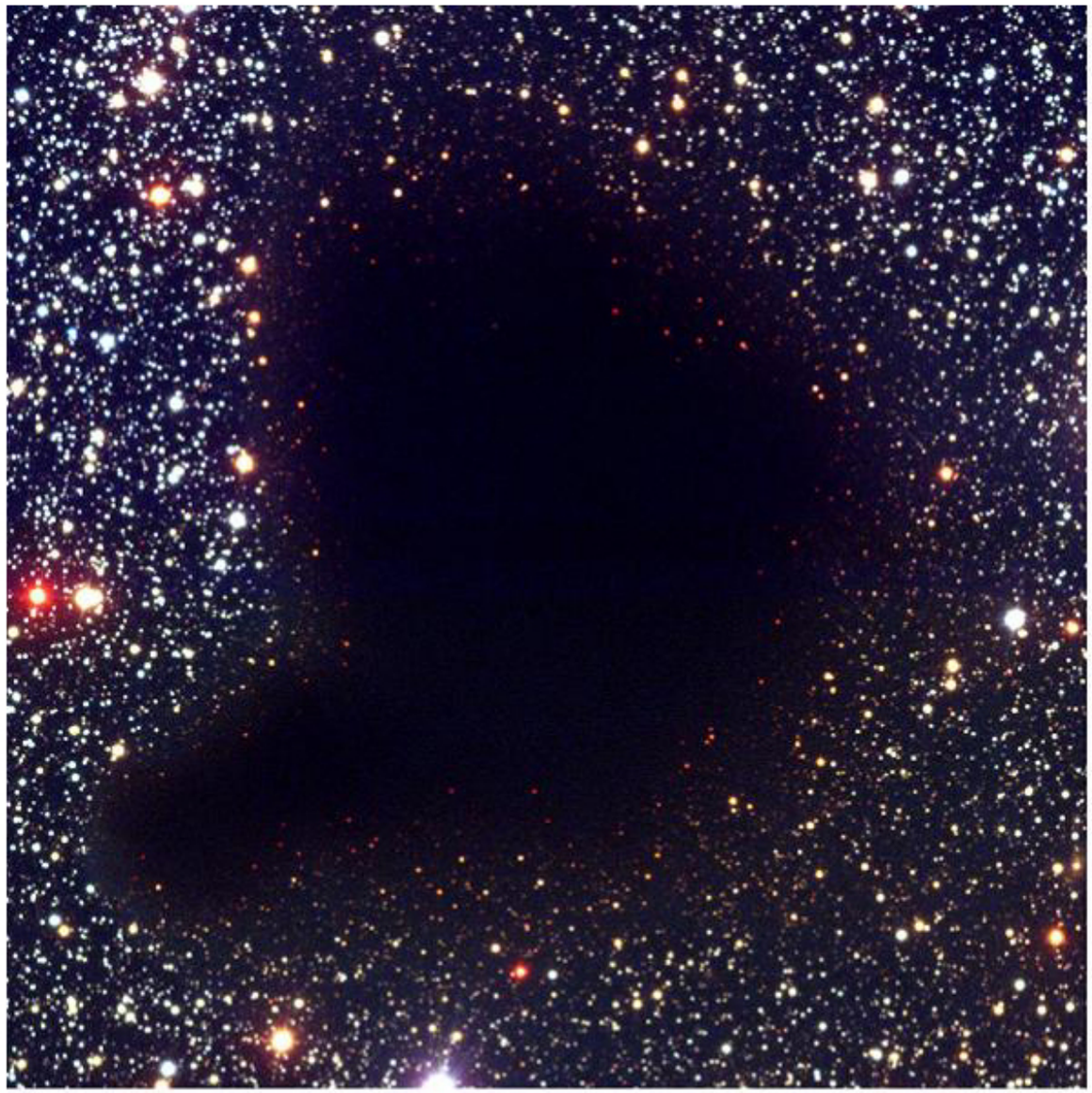

B, V, I

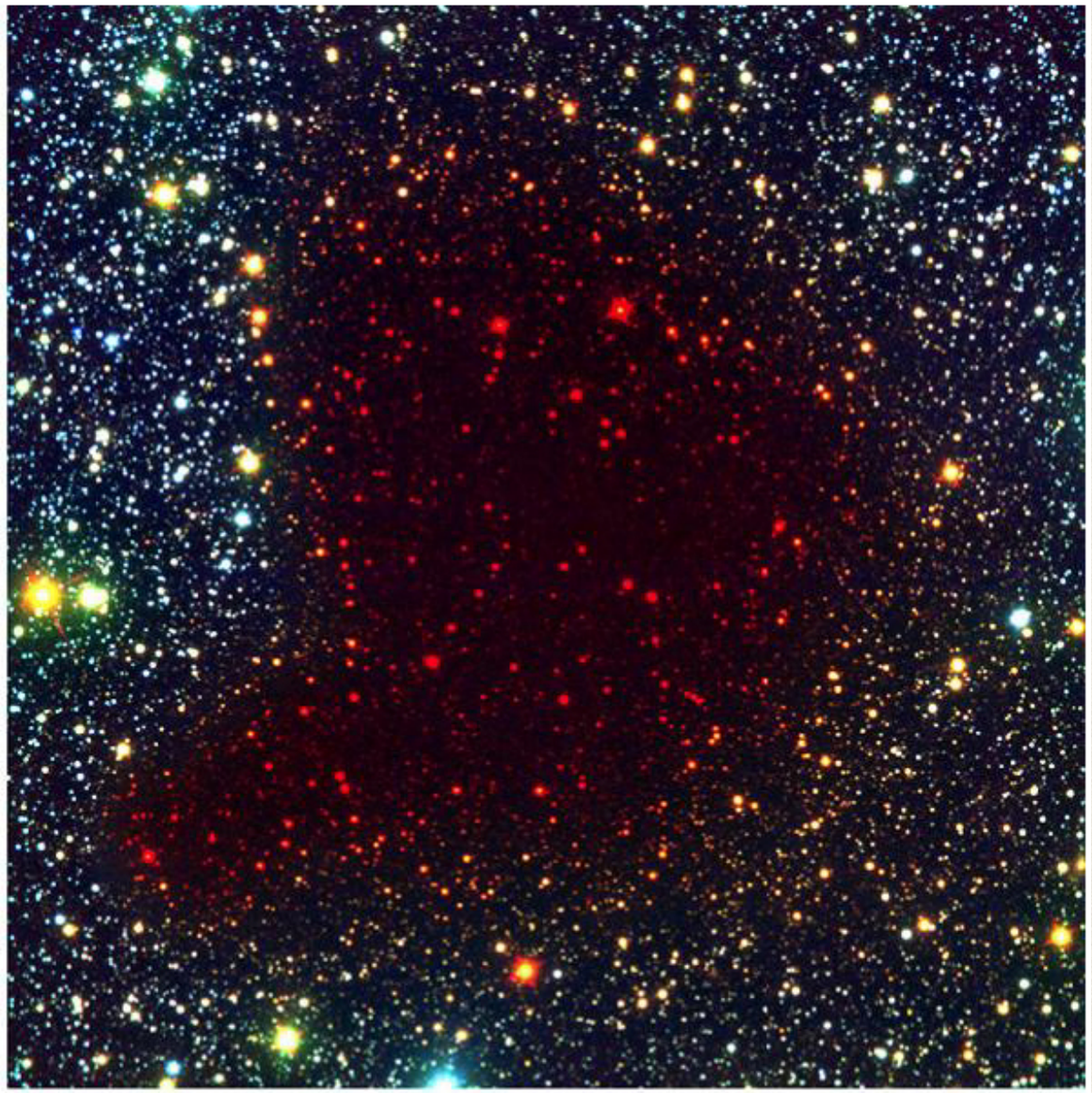

B, I, K

Pre-Collapse Black Cloud B68 (comparison)
(VLT ANTU + FORS 1 - NTT + SOFI)

ESO PR Photo 02c/01 (10 January 2001)

Example of a small dark cloud which absorbs the light of stars in the background.

Small dark clouds, as the one on the previous page have masses between $10^2 M_\Theta$ and $10^4 M_\Theta$ and radii between 1pc and 10pc. **Giant molecular clouds** on the other hand have sizes between 10pc and 60pc and masses from $10^5 M_\Theta$ to $10^{6.5} M_\Theta$.

The emission line widths of CO in molecular clouds are typically 3km/s and, so, much larger than the thermal velocities at T ≈ 30K. Therefore, the line width must be determined by turbulent velocities. One finds that the **velocity dispersion** σ_v correlates with the **size of the cloud** s like:

$$\sigma_v \approx 0.8 \frac{km}{s} \left(\frac{s}{pc} \right)^{0.5}$$

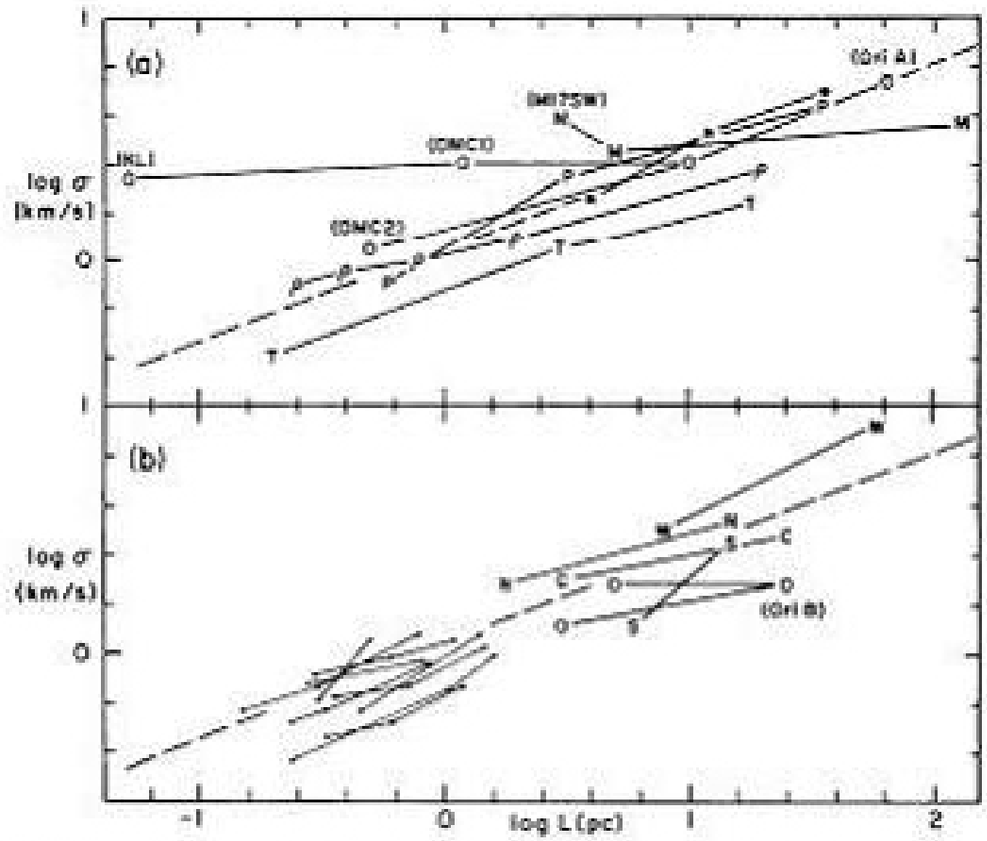

Figure 2. The velocity dispersion σ plotted versus region size L for clouds containing one or more subregions in Table 1. Straight lines connect the symbols for each subregion and the larger region or cloud of which it is a part. The data shown in the left part of panel (b) are from Snell (1979), and represent velocity dispersions inferred from the linewidth only. The dashed lines represent equation (1).

Larson 1981, MNRAS, 194, 809

As the pressure associated with the turbulent motions of the clouds is larger than the ambient pressure, it must be balanced by the gravitational attraction of the cloud itself. **Giant molecular clouds seem to be in approximate virial equilibrium.** For a mass M of a molecular cloud and a typical observed density profile like $\rho(r) = \bar{\rho} R / r$ (R = cloud radius), one obtains:

$$3M\sigma_v^2 = \frac{2}{3}\frac{GM^2}{R}$$

(magnetic fields being neglected). In numbers this reads:

$$M \approx 1000 M_\odot \frac{\sigma_v^2}{(km/s)^2}\frac{R}{pc}$$

Recall: $\sigma_v \approx 0.8 \frac{km}{s}\left(\frac{R}{pc}\right)^{0.5}$

This implies that the *mean column density* N_H of the clouds is approximately independent of their mass:

$$M/R^2 \approx N_H = 1.5 \cdot 10^{22}\, cm^{-2}$$

and their visual extinction is $A_V \approx 8$ mag (for a standard dust to gas ratio, see below).

Interstellar dust

Interstellar dust consists of tiny grains of silicates (much like ordinary beach sand or volcanic ash) and soot (very similar to the black soot in the exhaust of a diesel engine). The infrared emission spectra from dust in interstellar space are almost identical to the laboratory spectra of tiny grains of sand and soot.

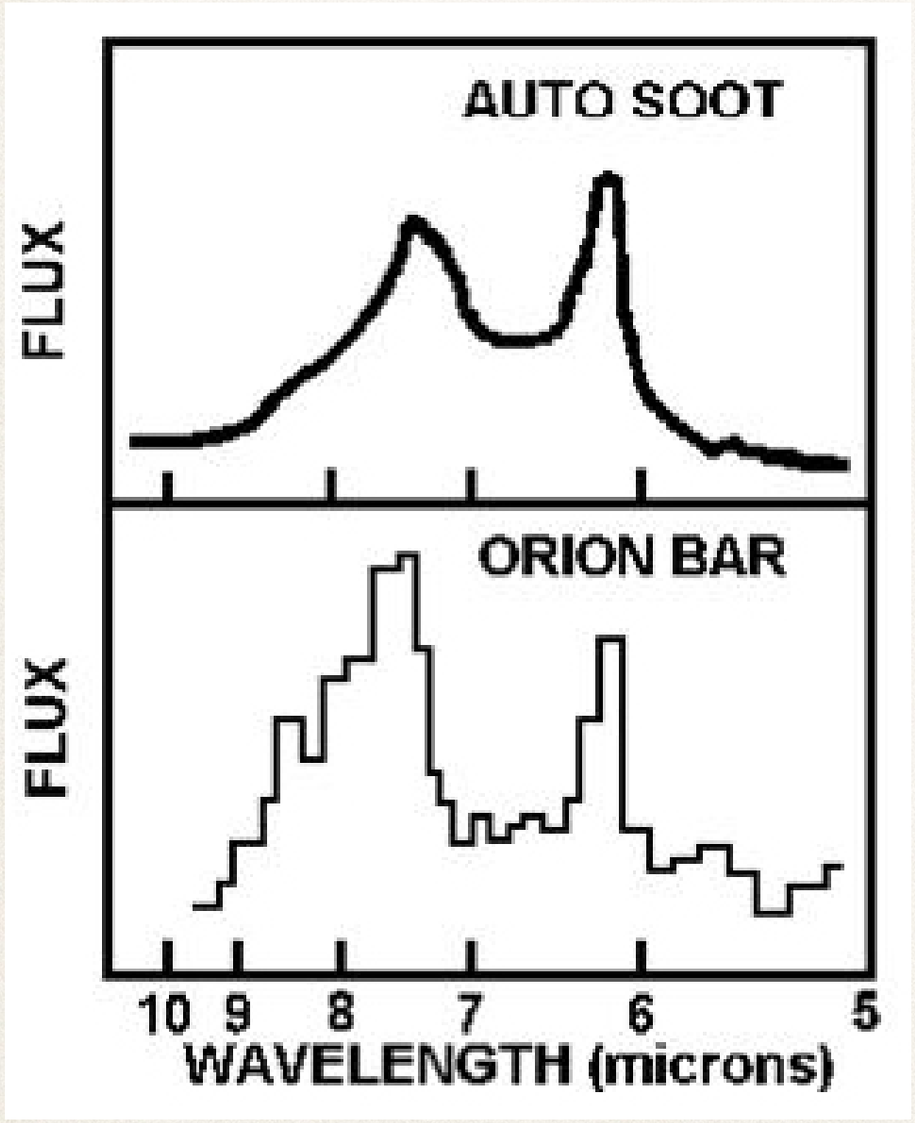

This graph shows a comparison of the infrared spectrum emitted by dust in the Orion Nebula (lower panel) and that emitted by the exhaust of a diesel truck (upper panel). Both spectra show prominent emission features at 6.2 and 7.6 micrometers that we can identify with the laboratory spectra of ”Polycyclic Aromatic Hydrocarbons”, or ”PAHs” – known carcinogens.

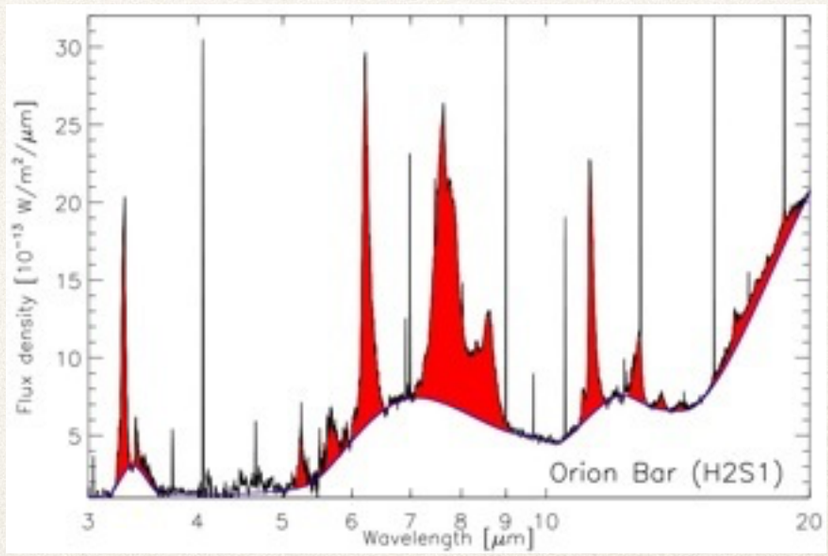

ISO-SWS spectrum of the Orion Bar, a very well known photodissociation region. Credits: E.Peeters

Photo-Dissociation Regions (PDRs)

- PAHs are mainly found in Photo-Dissociation Regions (PDRs)
- The most prominent PDRs are associated with gas that lies just outside of dense, luminous HII regions, and:
  - The pervasive WNM
  - Diffuse and translucent clouds
  - Reflection nebulae
  - Neutral envelopes around planetary nebulae
  - Photodissociated winds from red giant & AGB stars – The ISM in starburst galaxies & AGNs (NRL)
- PDRs include all ISM regions where the gas is predominantly neutral but where FUV photons play a significant role in the chemistry and/or the heating

(credits to J.R. Graham, UC Berkeley)

This image is a false-color composite where light detected at wavelengths of 0.43, 0.50, and 0.53 microns is blue. Light at wavelengths of 0.6, 0.65, and 0.91 microns is green. Light at 3.6 microns is orange, and 8.0 microns is red. (Credit NASA/Spitzer)

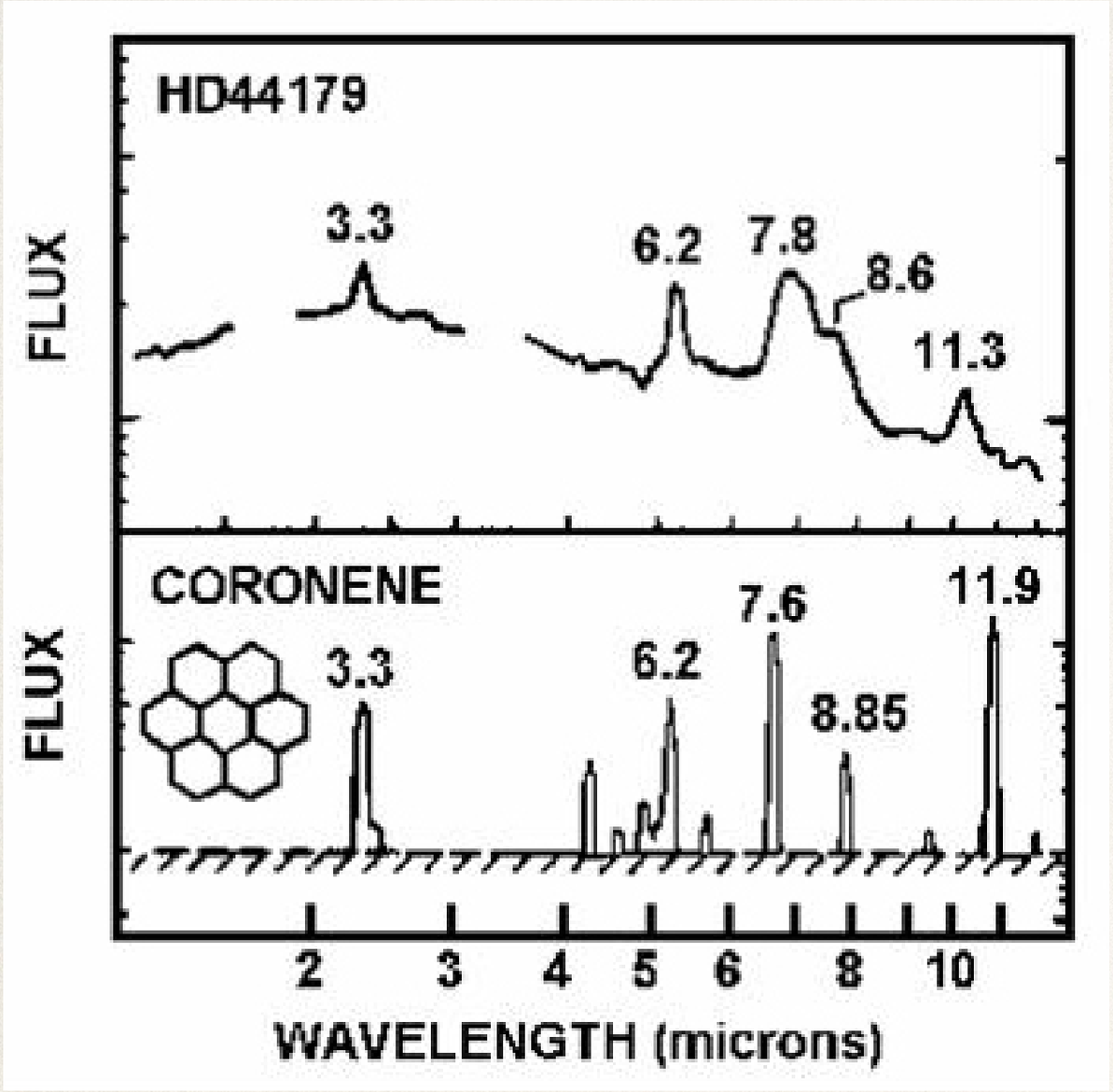

This graph compares the infrared spectrum from dust in the atmosphere of a red giant star (upper panel) with the laboratory spectrum of coronene, one type of ”Polycyclic Aromatic Hydrocarbons”. Observations with infrared spectrometers also show that the dust grains in the dense molecular clouds are often covered with ices, such as H_2O and CO_2 (dry ice).

Interstellar dust is produced in the outer atmospheres of red giant stars and expelled into interstellar space by these stars during the later stages of their evolution. We see in the figure above that the infrared spectrum of the red giant star HD44179 has emission features at 6.2 and 7.8 microns, just as does the spectrum of interstellar dust from the Orion Bar.

The interstellar dust grains are very effective absorbers of optical and ultraviolet radiation (but in radio, X-rays and infrared they aren't). The optical depth due to dust shows the following wavelength dependence:

$$\tau_{dust} \propto \lambda^{-1}$$

This behaviour is explained by **Mie scattering** at particles which have about the size of the wavelength of the scattered light (atoms or molecules are too small because then we would expect a dependence ~ λ^{-4}, i.e. Rayleigh scattering). As the scattered light from dust is partly polarized, the dust particles cannot be simply spherical.

As the dust is approximately distributed like the gas, column densities of HI (N_H) and extinction by dust (as measured by the absorption in the V-band A_V are well correlated. In the Milky Way we observe:

$$N_H = 1.9 \cdot 10^{21} A_V cm^{-2} mag^{-1}$$

Dust in star formation regions is exposed to strong radiation fields from hot massive stars. **The dust absorbes part of the incident UV radiation and reemits it at infrared wavelengths. This process is important for the cooling of star forming regions.**

(credits to Ralf Bender et al.)

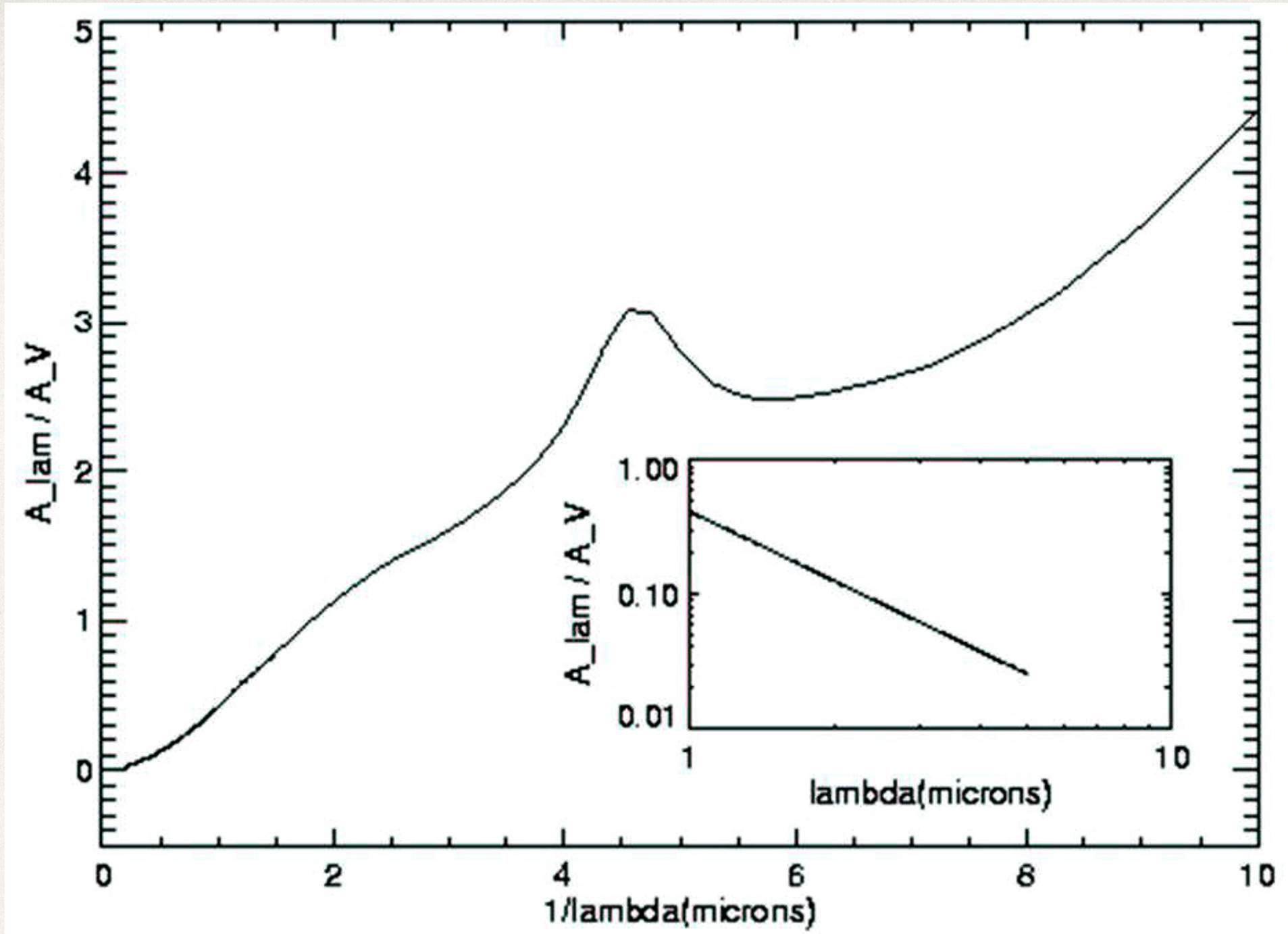

Averaged interstellar extinction curve A_λ according to Savage&Mathis (1979).

Fitting the FIR SED

- Dust emission approximated by

  - a blackbody curve $$B_\nu(T_\mathrm{d}) = \frac{2h\nu^3}{c^2}\frac{1}{e^{\frac{h\nu}{kT}}-1}$$

  - a modified (single temperature) blackbody $$f_\nu = \frac{M_\mathrm{d}}{D^2}\,\kappa_\mathrm{abs}\,B_\nu(T_\mathrm{d})$$

  - Multiple (modified) Black bodies

$$\kappa_\mathrm{abs} = \kappa_\mathrm{abs}(\lambda_0)\times\left(\frac{\lambda_0}{\lambda}\right)^\beta$$

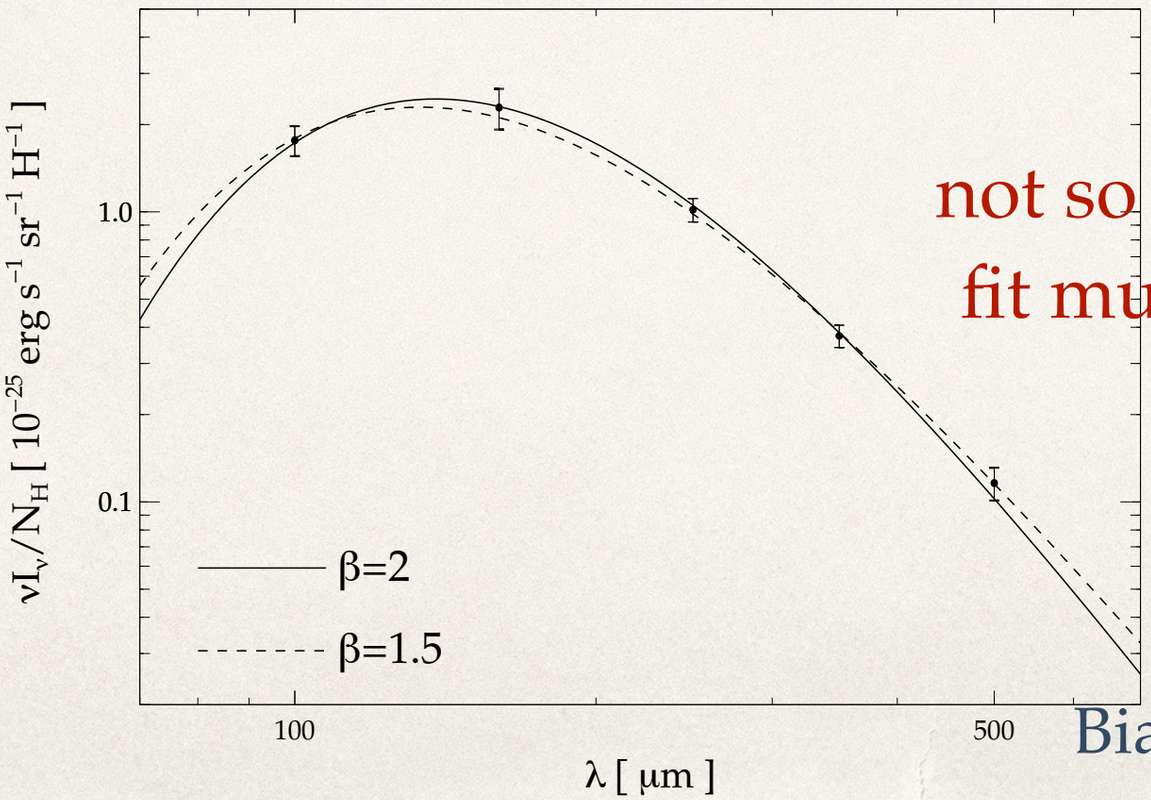

not so many datapoints to fit multiple components!

Bianchi (2013)

The energetic balance approach

- With MAGPHYS, da Cunha et al. (2008) have introduced a "fitting" method that imposes energy balance: what is lost in the UV-opt is what is emitted in FIR

- Limitations due to geometry: the absorbed and re-processed radiation is not necessarily re-emitted in the same direction!

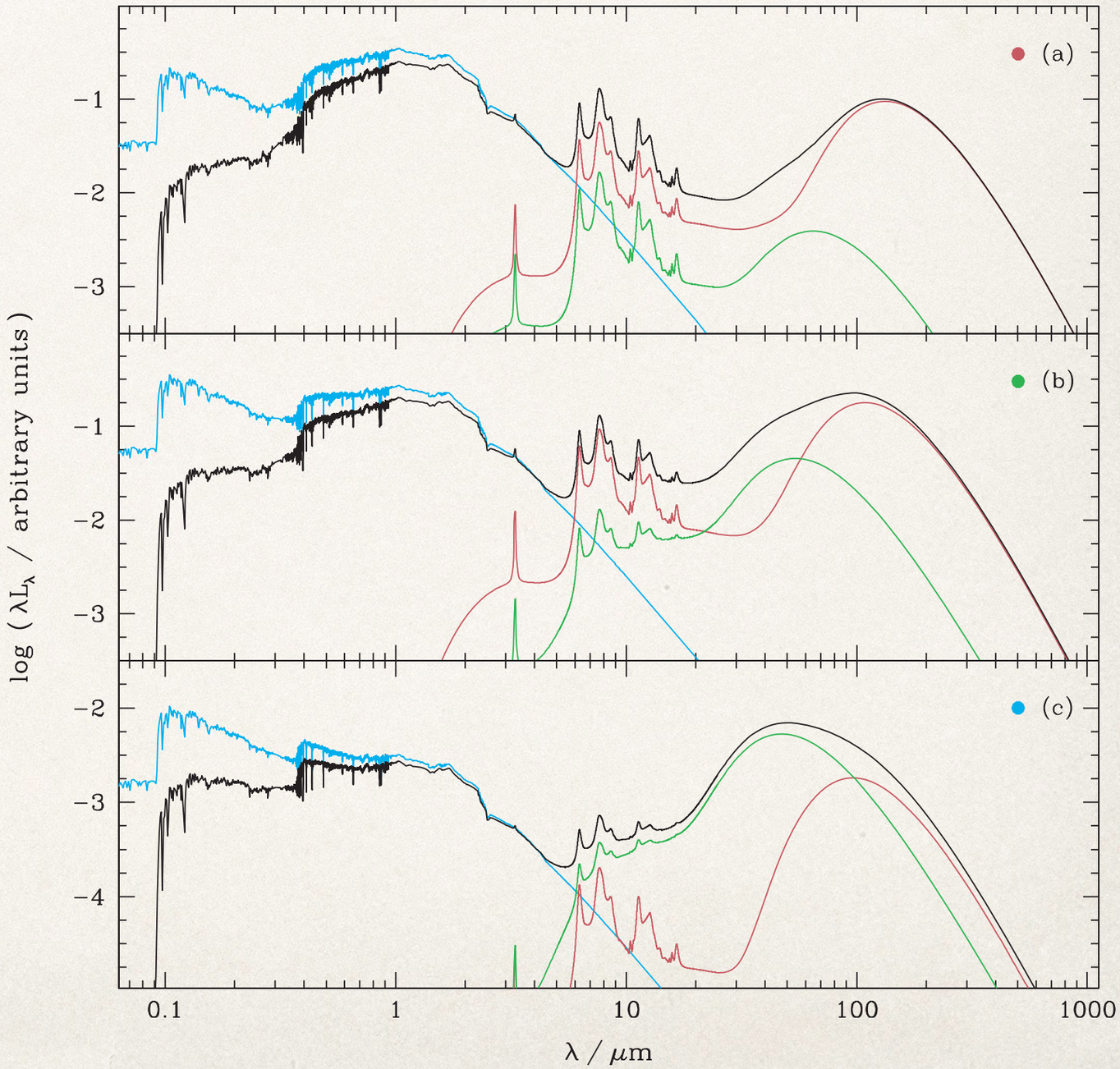

The "Schmidt-Kennicutt law"

$$\Sigma_{\rm SFR} = (2.5 \pm 0.7) \times 10^{-4} \left(\frac{\Sigma_{\rm gas}}{1\ M_\odot\ {\rm pc}^{-2}} \right)^{1.4 \pm 0.15} M_\odot\ {\rm yr}^{-1}\ {\rm kpc}^{-2}$$

$$\rho_{\rm SFR} \propto \frac{\rho_{\rm gas}}{(G\rho_{\rm gas})^{-0.5}} \propto \rho_{\rm gas}^{1.5}$$

dynamical argument

$$\Sigma_{\rm SFR} \propto \frac{\Sigma_{\rm gas}}{\tau_{\rm dyn}} \propto \Sigma_{\rm gas}\,\Omega_{\rm gas}$$

Kennicutt (1998, ApJ)

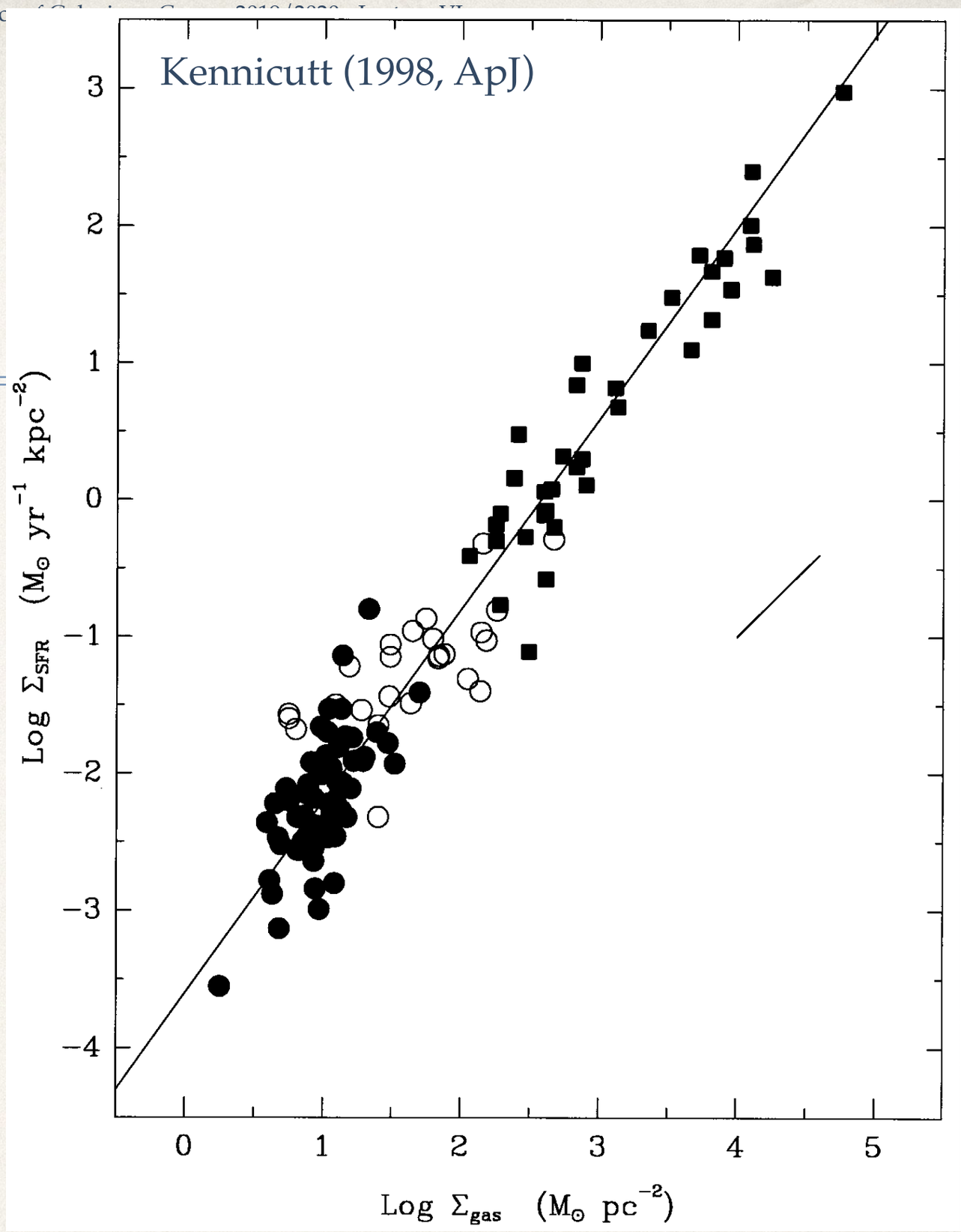

FIG. 6.—Composite star formation law for the normal disk (*filled circles*) and starburst (*squares*) samples. Open circles show the SFRs and gas densities for the centers of the normal disk galaxies. The line is a least-squares fit with index $N = 1.40$. The short, diagonal line shows the effect of changing the scaling radius by a factor of 2.

Is the S-K law unique and universal?

- Bigiel et al. (2008) find:
  $\Sigma_{SFR} \propto \Sigma_{H_2}$
- highlight 3 regimes
  - Starburst
  - "normal"
  - low density, HI - dominated: lot of scatter, changing from galaxy to galaxy — peculiar local conditions make the difference

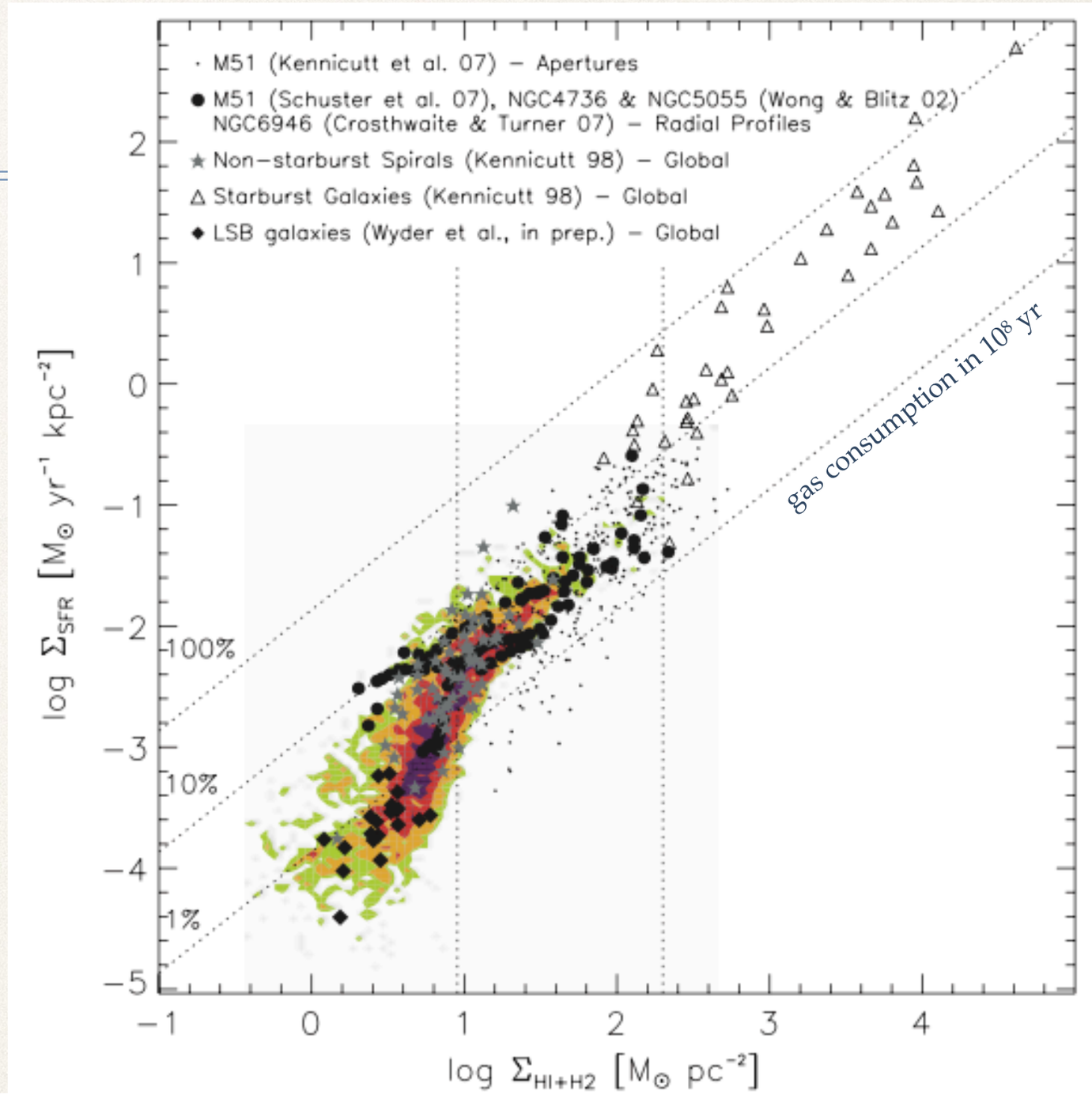

Figure 15. Σ_{SFR} vs. Σ_{gas} from this paper in colored contours (compare the middle-right panel of Figure 8) and for individual galaxies from other analyses (see Figure 14). The diagonal dotted lines and all other plot parameters are the same as in Figure 4. Overplotted as black dots are data from measurements in individual apertures in M51 (Kennicutt et al. 2007). Data points from radial profiles from M51 (Schuster et al. 2007), NGC 4736, and NGC 5055 (Wong & Blitz 2002) and from NGC 6946 (Crosthwaite & Turner 2007) are shown as black filled circles. Furthermore, we show disk-averaged measurements from 61 normal spiral galaxies (filled gray stars) and 36 starburst galaxies (triangles) from K98. The black filled diamonds show global measurements from 20 low surface brightness galaxies (Wyder et al. 2008). Data from other authors were adjusted to match our assumptions on the underlying IMF, CO line ratio, CO-to-H_2 conversion factor and galaxy inclinations where applicable. One finds good qualitative agreement between our data and the measurements from other studies despite a variety of applied SFR tracers. This combined data distribution is indicative of three distinctly different regimes (indicated by the vertical lines) for the SF law (see discussion in the text).